THE ASTROPHYSICAL JOURNAL, 289:173–187, 1985 February 1

FORCE-FREE EQUILIBRIA OF MAGNETIZED JETS

ARIEH KÖNIGL[1] AND ARNAB RAI CHOUDHURI[2]
The University of Chicago
Received 1984 May 29; accepted 1984 August 13

ABSTRACT

We study the equilibrium configurations of magnetized, supersonic jets that are confined by a slowly varying external pressure. We concentrate on magnetic-pressure-dominated jets, in which the mean field satisfies the force-free equation $\nabla \times \boldsymbol{B} = \mu \boldsymbol{B}$. If the jets are somewhat dissipative, then μ will be constant across the jet and will change only slowly along the jet. In jets with a high magnetic Reynolds number, the global topological properties of the field lines will be preserved while the jet settles to a minimum-energy configuration. In particular, the magnetic helicity (which is a measure of the twist and knottedness of the field lines) should be an approximately conserved quantity. Under these conditions, the minimum-energy solution of the field equation is in general a linear superposition of only two modes: an axisymmetric mode which accounts for the net flux and axial current in the jet, and a helical mode which varies along the jet with a wavelength $\lambda \approx 5R$ (where R is the jet's radius). The nonaxisymmetric mode becomes energetically favorable when the external pressure drops below a certain critical value, given by $2.7 \times 10^3 \tilde{K}^4 \Psi^{-6}$ (where $\tilde{K}$ is the magnetic helicity per unit length, and Ψ is the magnetic flux). This behavior has been observed, under analogous conditions, in laboratory experiments on reversed-field pinches, and it appears to be a general property of dynamical systems in which a dissipation mechanism acts selectively on different integrals of motion (in this case, magnetic energy and helicity).

This model is applied to the interpretation of the total and the polarized emission from resolved jets observed at a large angle to the axis. (An application to unresolved jets observed at a small angle to the axis is considered in the companion paper on BL Lacertae objects.) The model can account for the various nonaxisymmetric features of extended jets like NGC 6251, including the oblique orientations of projected magnetic field vectors and of Faraday rotation-measure gradients with respect to the jet axis, and the apparent transverse oscillations of the ridge line which do not involve the outer isophotes. The model also explains the observed oscillations of the FWHM and of the degree of polarization along the jet as well as the general appearance of emission knots. We point out a number of specific observational predictions that follow from this interpretation. In addition, we briefly explore the possibility that the magnetic energy which must be dissipated during the expansion of a force-free jet to maintain a minimal field configuration is the main source of energy for the observed synchrotron emission.

Subject headings: galaxies: jets — hydromagnetics — polarization — radiation mechanisms

I. INTRODUCTION

The possible influence of embedded magnetic fields on the dynamical evolution of extragalactic radio jets has been recognized already in early models of these sources. Blandford and Rees (1974) noted that, in a nonrelativistic, supersonic jet which convects a "frozen-in" magnetic field, the magnetic pressure associated with the transverse field component would scale with the jet radius R as R^{-2}, slower than either the longitudinal field pressure ($\propto R^{-4}$) or (in a nonisothermal jet) the thermal pressure ($\propto R^{-2\Gamma}$, where Γ is the adiabatic index). They therefore inferred that, in jets where R increases to a sufficiently large value, the *transverse* dynamics of the flow may become dominated by magnetic stresses even if it were previously controlled by thermal effects. The establishment of a predominantly transverse field configuration sufficiently far out along the jet, which was predicted by this argument, has subsequently been inferred from polarization measurements in a number of jets associated with low-luminosity radio galaxies (e.g., Bridle and Perley 1984), and has motivated a closer examination of the dynamical role of the magnetic field. One effect which has been examined in this connection in some detail is the possible magnetic self-confinement of the jet (Chan and Henriksen 1980; Bicknell and Henriksen 1980; Bridle, Chan, and Henriksen 1981). In this picture, if the jet carries a net current (as originally proposed by Benford 1978), then the hoop stresses exerted by the associated toroidal field will eventually cause a divergent flow to recollimate. Under adiabatic conditions, the subsequent compression will raise the thermal pressure in the jet to a point where the contraction is reversed. The radius of the jet will thus oscillate with an amplitude that depends on the internal Alfvén Mach number and on the external pressure run. This model has been applied to the interpretation of the observed oscillations of the FWHM in several radio jets (e.g., Bridle *et al.* 1980).

The Chan and Henriksen (1980) model of magnetically induced oscillations is based on the assumption that after the magnetic stresses become dynamically important, they remain in approximate equipartition with the thermal pressure in the jet. It is clear, however, that if radiative losses can prevent the thermal pressure from rising too rapidly when the jet is compressed, or if the jet carries very little net current in the first place, then the ratio of the magnetic pressure to the thermal pressure will continue to grow.

[1] Department of Astronomy and Astrophysics.
[2] Department of Physics.

(It is even conceivable that in some jets this ratio is already greater than unity at the origin of the outflow.) Under these conditions, the convected magnetic field lines may be expected to rearrange themselves and approach a *force-free* configuration, with the current density $\nabla \times \boldsymbol{B}$ being nearly everywhere parallel to the magnetic field $\boldsymbol{B}$ (e.g., Rees, Begelman, and Blandford 1981). Such a configuration will be different from the axisymmetric, self-similar field structure considered in the Chan and Henriksen (1980) model (see also Blandford and Payne 1982). In particular, it need not be axisymmetric. There is now evidence from high-resolution polarization maps of jets such as NGC 6251 (Perley, Bridle, and Willis 1984) for the repeated occurrence of *oblique* projected field orientations along the jet which cannot be explained with axisymmetric models. In the latter source, other observed features are also nonaxisymmetric, including the projected directions of the Faraday rotation-measure (RM) gradients across the jet, and the lateral oscillations of the intensity ridge line. The most plausible mechanism which has previously been suggested for causing such oscillations is the helical ($m = 1$) mode of the Kelvin-Helmholtz instability. However, for the relatively high Mach number and external-to-internal density ratio inferred for this jet, the wavelength of this mode should be much larger than the jet radius (e.g., Ferrari, Trussoni, and Zaninetti 1983), whereas the lateral oscillations (as well as the variations in the projected field directions and in the RM gradients) are found to occur on a scale of only a few times the apparent diameter of the jet.

In this paper we study the force-free equilibria of magnetic-pressure-dominated, supersonic jets which are confined by a slowly varying external pressure. We demonstrate that, if the jets possess an internal dissipation mechanism, then the lowest-energy magnetic field configuration will in general be a superposition of two modes, one axisymmetric and one helical (of wavelength $\lambda \approx 5R$). We show that the nonaxisymmetric mode dominates when either the net magnetic flux in the jet is small or the external pressure is low, and that the synchrotron emission then exhibits the nonaxisymmetric features that are observed in jets like NGC 6251. We are thus able to account for these phenomena in a natural way as a consequence of the *equilibrium* structure of the jet, without having to invoke any instabilities.

In our discussion of the equilibrium properties of magnetized jets, we are guided, to a large extent, by the results of laboratory experiments on the so-called diffuse, reversed-field pinches and by their theoretical interpretations. Such experiments generally consist of establishing an axial field in a stationary plasma column by means of external coils, and then passing a current in the plasma which creates a toroidal field. After an initially turbulent and dissipative phase, it is often observed that the plasma settles into a quiescent, stable state which is characterized by a reversed axial field in the outer regions of the column. It has also been reported that, if the ratio of the induced current to the applied axial field is sufficiently large, then the relaxed field configuration is nonaxisymmetric (e.g., Bodin and Newton 1980). The original interpretation of these observations in terms of force-free fields was given by Taylor (1974, 1975), who pointed out that both the field reversal and the break of axial symmetry in the final equilibrium state may be attributed to the conservation of magnetic helicity in the plasma. The concept of magnetic helicity (the volume integral of the dot product of the magnetic vector potential and the magnetic field) has since been central to the theory of reversed-field pinches, and it remains a key concept also in our application. Although magnetic helicity is an approximately conserved quantity in highly conducting flows (see Appendix A), the possible consequences of this fact in jets have not yet been discussed in the literature.

The plan of this paper is as follows: In § II we apply a variational principle to derive the general form of the force-free field configuration in the jet and discuss its dependence on the various relevant parameters. In § III we first calculate the total and the polarized synchrotron intensities for several representative magnetic field geometries, and then we use the results to interpret various aspects of resolved jets (such as NGC 6251) observed at a large angle to the axis. (The emission from unresolved jets observed at a small angle to the axis is considered in the companion paper [Königl and Choudhuri 1985].) We summarize our conclusions in § IV.

II. FORCE-FREE EQUILIBRIA

a) The Magnetic Field Equation

Consider a magnetic-pressure-dominated jet of velocity $\boldsymbol{v}_j$ and density ρ_j which is confined laterally by the pressure of a highly conducting external medium of density ρ_e. We suppose that the magnitude of the "frozen-in" magnetic field $\boldsymbol{B}$ everywhere satisfies $B^2 < 4\pi\rho_j v_j^2$, so that the jet is super-Alfvénic (Alfvén Mach number $M_A > 1$), and we assume that the flow is also supersonic with respect to the ambient medium (Mach number $M_e > 1$). Associated with the magnetic field is a vector potential $\boldsymbol{A}$ satisfying $\nabla \times \boldsymbol{A} = \boldsymbol{B}$, and one can define the *magnetic helicity* of the jet by

$$K \equiv \frac{1}{8\pi} \int_{V_j} \boldsymbol{A} \cdot \boldsymbol{B} dV_j , \tag{1}$$

where V_j denotes the comoving volume of the jet. For a volume bounded by a magnetic surface, one can show quite generally that K is a measure of the twist and knottedness of the enclosed magnetic field lines (Berger and Field 1984; see also Moffatt 1978). The helicity is thus a topological property of the field lines and, hence, must be conserved if the jet is a perfect conductor which convects the field in a continuous manner. We demonstrate this fact formally in Appendix A. Since the jet will, in general, have a variable cross section, we find it more convenient to consider the helicity *per unit length* (which we denote by $\tilde{K}$) rather than the total helicity K. As discussed in Appendix A, this quantity will be constant along the jet if the flow is super-Alfvénic and if, as we shall henceforth assume, the velocity $\boldsymbol{v}_j$ and the rate of injection of magnetic helicity at the origin of the jet are effectively constant.

The conservation of helicity constitutes a topological constraint which determines the equilibrium structure of the magnetic field in the rest frame of the jet. This structure can be derived from a variational principle, which consists of minimizing the specific magnetic energy in the jet,

$$\tilde{W} = \frac{1}{8\pi} \int_{\tilde{V}_j} B^2 d\tilde{V}_j \tag{2}$$

(where $\tilde{V}_j$ is the comoving volume per unit length), subject to the constraint $\tilde{K} = \text{const}$. As was first shown by Woltjer (1958), this procedure leads to a solution of the form

$$\nabla \times \boldsymbol{B} = \mu \boldsymbol{B} , \tag{3}$$

where μ is locally a constant. This is a special case of the force-free solution. The general form of the force-free solution, which corresponds to μ in equation (3) being any function of the coordinates that satisfies $\boldsymbol{B} \cdot \nabla \mu = 0$, can be derived from the same variational principle by considering a perfectly conducting plasma which contains an arbitrary collection of closed magnetic field lines and magnetic surfaces. In this case, the magnetic helicity is conserved separately for each volume element bounded by field lines, so the variational procedure implies that μ must be constant on each one of these loops or surfaces; however, the value of the constant may vary from one field line to another. The derivation of equation (3) is thus seen to involve the assumption that the boundary of the jet is effectively the only magnetic surface which needs to be considered in the variational process, or, equivalently, that each magnetic field line in the jet may for this purpose be regarded as following a volume-filling path. This situation might arise if the plasma in the jet were *not* perfectly conducting. In this view (Taylor 1974, 1975; Rusbridge 1977; Jacobson and Moses 1984), small departures from perfect conductivity lead to local breaking and reconnection of field lines throughout the volume of the plasma which destroy the topological properties of individual field lines but preserve the global invariant given by equation (1). The dissipation of magnetic energy which necessarily accompanies all such changes in the field topology is consistent with the decrease in $\tilde{W}$ that is envisioned in the variational principle. In fact, one may give a physical description of the processes postulated in the derivation of equation (3) in terms of magnetohydrodynamic (MHD) *turbulence*. This was pointed out by Montgomery, Turner, and Vahala (1978), who noted that in three-dimensional MHD turbulence, energy cascades to lower spectral scales where it may be dissipated, whereas magnetic helicity cascades to larger scales where dissipation is relatively slow. Using this approach, Turner (1983*a*, *b*) has constructed a statistical model of a magnetized fluid in which equation (3) describes the structure of the *mean* field in the plasma.

We have belabored the physical interpretation of equation (3) to strengthen the argument in favor of its applicability to extragalactic jets. In particular, we note that these jets are generally believed to have rather high Reynolds numbers (e.g., Henriksen, Bridle, and Chan 1982), so that they may well be turbulent. We wish to stress, however, that the reasons for expecting a force-free solution with a constant μ are quite general and are not tied to the specific mechanism through which this state is attained. Essentially, what is required is some efficient mode of dissipation which would allow the jet to approach its minimum-energy configuration. As noted in § I, the adiabatic expansion of the jet tends to lower its thermal pressure p_j relative to the magnetic pressure $B^2/8\pi$, and if radiative cooling can prevent any magnetic pinch stresses that may be present from increasing p_j to the equipartition value, then the jet should eventually become force free. This is simply a consequence of the hydrostatic balance condition, $\nabla p_j = (\nabla \times \boldsymbol{B}) \times \boldsymbol{B}/4\pi$, in the jet. (Note, however, that even though the thermal pressure *gradients* are expected to become negligibly small, p_j itself could remain finite.) In addition, it can be shown explicitly that, in the presence of dissipation, the only time-independent, force-free configuration is the one with $\mu = \text{const}$. (see Jette 1970). Thus, one can argue directly that equation (3) should describe the steady-state topology of a magnetized, imperfectly conducting jet. In § III*b*, we briefly consider the question of whether the observed synchroton emission from radio jets can account for the energy dissipated in the field-redistribution process. Here we merely postulate that an efficient dissipation mechanism does exist and proceed to examine the consequences.

b) Solution of the Field Equation

The general solution of equation (3) in cylindrical coordinates can be written as a series of the form $\boldsymbol{B} = \Sigma_{m,k}\, B_{mk}\, \boldsymbol{b}^{mk}(r, \theta, z)$, where m is a nonnegative integer, and where the individual modes $\boldsymbol{b}^{mk}$ depend on θ and z through the phase function $\phi \equiv (m\theta + kz)$ (Chandrasekhar and Kendall 1957; Barberio-Corsetti 1973). The explicit expressions for the modes generally involve a linear combination of the Bessel functions J_m and the Neumann functions N_m; however, when the domain of the solution includes the axis $r = 0$ (as in the case of a filled jet), these expressions simplify to

$$\begin{aligned} b_r^{mk} &= -\frac{1}{(\mu^2 - k^2)^{1/2}} \left[kJ_m'(y) + \frac{m\mu}{y} J_m(y) \right] \sin \phi , \\ b_\theta^{mk} &= -\frac{1}{(\mu^2 - k^2)^{1/2}} \left[\mu J_m'(y) + \frac{mk}{y} J_m(y) \right] \cos \phi , \\ b_z^{mk} &= J_m(y) \cos \phi , \end{aligned} \tag{4}$$

where $y \equiv (\mu^2 - k^2)^{1/2} r$, and where the prime denotes differentiation with respect to the argument.

The boundary condition that must be satisfied by this solution in the case of a perfectly conducting external medium is that the normal component of $\boldsymbol{B}$ vanish. (In the case of a resistive jet confined by a good conductor, the surface current density must also vanish, so the field cannot remain force-free at the boundary.) If the jet surface is a cylinder of radius R, then the condition on the normal component of $\boldsymbol{B}$ becomes $B_r(R) = 0$. This condition is automatically satisfied by the $m = 0$, $k = 0$ mode, but for all other modes it leads to an eigenvalue equation which relates μ to m and k. In this geometry, the $m = 0$, $k = 0$ mode is also the only one which accounts for a net axial flux (or, equivalently, a net axial current) in the plasma.

In § II*a* we noted that equation (3) can be derived from a variational principle in which the specific magnetic energy $\tilde{W}$ is minimized subject to the constraint that the specific magnetic helicity $\tilde{K}$ remain constant. It does *not* follow, however, that in any given field arrangement with a prescribed value of $\tilde{K}$, all modes contribute equally to $\tilde{W}$. Taylor (1974, 1975) first pointed out the rather surprising fact that, in a cylindrical geometry, the most general minimum-energy configuration which satisfies the boundary condition consists of only the $m = 0$ and $m = 1$ modes, and of no other mode! Taylor derived this result in connection with his

interpretation of diffuse pinch discharges in cylindrical plasma columns bounded by perfectly conducting, *rigid* walls (see § I). It may thus appear at first sight unlikely that a similar result would apply to astrophysical jets which are not confined by a rigid boundary, but rather by the pressure of an external medium (i.e., the boundary is *free*). Taking, for example, the $m = 1$ mode, it is seen from equation (4) that its contribution to the pressure at $r = R$ oscillates between the peak value and zero on going halfway around the boundary (at constant z), or half a wavelength along the boundary (at constant θ). For a free boundary under static conditions, this behavior would cause large distortions away from cylindrical geometry.

In spite of these apparent caveats, it turns out that, for a magnetically dominated jet confined by a uniform or slowly varying external pressure and satisfying M_A, $M_e \gg 1$, the approximation of an effectively rigid, cylindrical boundary is justified. The slow variation of the pressure ensures that the *mean* jet radius R remains nearly constant over a length scale much larger than R. In fact, for a confined jet, $dR/dz \lesssim 1/M_A$, so the cylindrical approximation should be adequate as long as $M_A \gg 1$. The requirement $M_e \gg 1$, on the other hand, guarantees that the deviations from the mean radius remain small. This can be seen by considering the ripples ΔR induced at the surface of the jet by the periodic pressure variations of the $m > 0, k > 0$ modes of equation (4), and by analyzing either the response of the external medium to the passage of these ripples or the force-balance condition in the rest frame of the jet. By either method, one finds $\Delta R/R \lesssim 1/M_e$ (see Appendix B). Physically, this result reflects the fact that the relative supersonic motion endows the ambient medium with an effective rigidity which inhibits large variations in R even though the boundary of the jet is free. This conclusion is valid regardless of whether $\eta \equiv \rho_j/\rho_e$ is greater than or less than unity, although for $\eta < 1$ the jet could be effectively rigid ($M_e \gg 1$) and yet have a relatively low value of M_A which would allow it to adjust rapidly to any variations in the external pressure. (A jet with $\eta < 1$ is also less susceptible to Kelvin-Helmhotz instabilities; e.g., Ferrari, Trussoni, and Zaninetti 1983.)

When the above conditions are satisfied, one may approximate any given portion of the jet where $p_e \approx$ const. by a cylinder of mean radius R. This radius can be calculated from equation (4) by equating p_e with the mean magnetic pressure (the value of $[B_\theta^2 + B_z^2]/8\pi$ averaged over θ) at $r = R$. To the extent that the surface ripples ΔR can be neglected ($M_e \gg 1$), the boundary condition is again $B_r(R) \approx 0$, and Taylor's conclusions regarding the lowest energy field configuration should apply. We now demonstrate this result explicitly in the context of a pressure-confined jet.

c) *The Minimum-Energy State*

We wish to determine the lowest energy configuration of a cylindrical, $v_j =$ const. jet as a function of the magnetic helicity per unit length $\tilde{K}$, the net axial flux Ψ, and the external pressure p_e. Starting from equation (2) and using the identity $\boldsymbol{B} \cdot \nabla \times \boldsymbol{A} = \boldsymbol{A} \cdot \nabla \times \boldsymbol{B} + \nabla \cdot \boldsymbol{A} \times \boldsymbol{B}$ as well as equation (3) and Stokes's theorem, we can express the magnetic energy per unit length in terms of $\tilde{K}$ by

$$\tilde{W} = \mu\tilde{K} + \frac{1}{8\pi}\int_{\Sigma_j} \boldsymbol{A} \times \boldsymbol{B} \cdot d\boldsymbol{\Sigma}_j \equiv \mu\tilde{K} + S\,, \tag{5}$$

where Σ_j denotes the jet's surface area per unit length (cf. Reiman 1980). If one employs the Chandrasekhar-Kendall representation (eq. [4]), then only the $m = 0, k = 0$ mode contributes to the surface integral. This mode is given by

$$B_r^{\,0} = 0\,, \qquad B_\theta^{\,0} = B_0 J_1(\mu R)\,, \qquad B_z^{\,0} = B_0 J_0(\mu R) \tag{6}$$

(see Fig. 1), and is also the only one which contributes to the net axial flux,

$$\Psi = \frac{2\pi B_0 R^2}{\mu R} J_1(\mu R)\,. \tag{7}$$

(Henceforth, we suppress the k-dependence in the amplitudes $\boldsymbol{b}^{mk}$. For the $m = 0$ mode, the requirement that the field be divergence free implies that k must also be zero.) If $\boldsymbol{A}$ is defined so that $A_\theta(R) = \Psi/2\pi R$ and $A_z(R) = 0$ (see Appendix A), then it is straightforward to verify that, in equation (5),

$$S = \left(\frac{\Psi}{4\pi}\right)^2 \frac{\mu R}{R^2} \frac{J_0(\mu R)}{J_1(\mu R)}\,, \tag{8}$$

and

$$\tilde{K}_0 = \left(\frac{\Psi}{4\pi}\right)^2 \frac{1}{R}\left\{\frac{\mu R[J_0^{\,2}(\mu R) + J_1^{\,2}(\mu R)] - 2J_0(\mu R)J_1(\mu R)}{J_1^{\,2}(\mu R)}\right\}. \tag{9}$$

As long as only the $m = 0$ mode is present, the radius R is given from the pressure-balance condition by

$$R = \left\{\frac{(\mu R)^2}{2\pi p_e}\left(\frac{\Psi}{4\pi}\right)^2\left[1 + \frac{J_0^{\,2}(\mu R)}{J_1^{\,2}(\mu R)}\right]\right\}^{1/4}. \tag{10}$$

It is clear from equations (9) and (10) that the combinations $F_0 \equiv \tilde{K}_0 R/\Psi^2$ and $G_0 \equiv p_e R^4/\Psi^2$ define two dimensionless quantities which are functions of μR alone. One can eliminate R between F_0 and G_0 by defining the function $H_0(\mu R) \equiv p_e \Psi^6/\tilde{K}_0^{\,4} = G_0/F_0^{\,4}$, which can then be used to calculate μR for the given values of $\tilde{K}_0$, Ψ, and p_e. After obtaining μR, one can derive the values of R, S, and $\tilde{W}_0$ by a successive application of equations (10), (8), and (5).

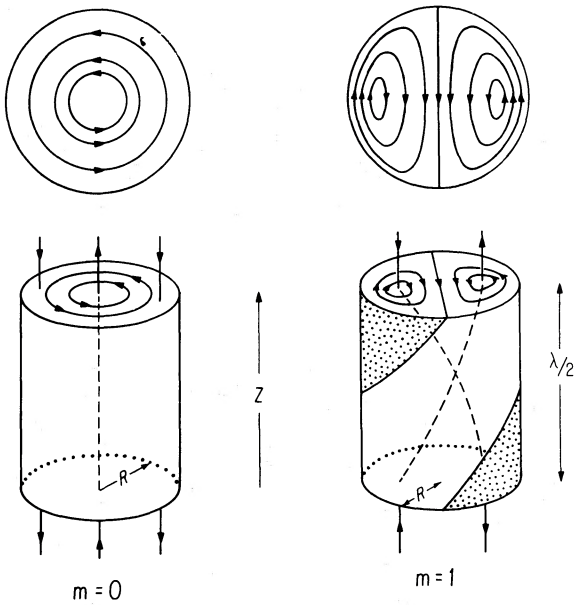

FIG. 1.—Schematic representation of the magnetic field configuration in the $m = 0$ and $m = 1$ modes. In each case, the upper diagram shows a cross section normal to the jet axis, while the lower diagram gives a side view of the jet. The arrows indicate the directions of the local magnetic field vectors, whereas the dashed curves trace the loci of neutral points (i.e., points where $B_r = B_\theta = 0$) in successive cross sections. The $m = 0$ field configuration is axisymmetric, with the axial component B_z decreasing away from the axis and possibly changing sign near the boundary. The $m = 1$ field configuration is helical (wavelength $\lambda \approx 5R$), and corresponds to two oppositely directed flux tubes (one of which is stippled in the illustration) that are wrapped around each other. In this case, B_z vanishes on the axis.

A similar procedure can be used to calculate R and $\tilde{W}$ when both the $m = 0$ *and* the $m = 1$ modes are present. Using the identity $J_1'(y) = J_0(y) - J_1(y)/y$, and defining the amplitude-ratio ϵ by $B_1 \equiv \epsilon B_0$, we rewrite the $m = 1$ field components in the form

$$B_r^{\,1} = -\frac{\epsilon B_0}{(\mu^2 - k^2)^{1/2}}\left[kJ_0(y) + \frac{(\mu - k)}{y}J_1(y)\right]\sin(\theta + kz)\,,$$

$$B_\theta^{\,1} = -\frac{\epsilon B_0}{(\mu^2 - k^2)^{1/2}}\left[\mu J_0(y) - \frac{(\mu - k)}{y}J_1(y)\right]\cos(\theta + kz)\,,$$

$$B_z^{\,1} = \epsilon B_0 J_1(y)\cos(\theta + kz)\,, \tag{11}$$

where again $y \equiv (\mu^2 - k^2)^{1/2}r$ (see Fig. 1). In order to calculate the contribution of this mode to the magnetic helicity, we must take account of the boundary condition $B_r(R) = 0$, which implies

$$kRJ_0(Y) + \left(\frac{\mu R - kR}{\mu R + kR}\right)^{1/2}J_1(Y) = 0\,, \tag{12}$$

where $Y \equiv [(\mu R)^2 - (kR)^2]^{1/2}$. The result is

$$\tilde{K}_1 = \frac{\epsilon^2}{R}\left(\frac{\Psi}{8\pi}\right)^2 \frac{\mu R(\{2\{(\mu R)^2[1 + (kR)^2] - (\mu R)(kR)\}(\mu R + kR)^2 - (\mu R - kR)^2\}J_0^{\,2}(Y) + (\mu R - kR)^2)}{Y^4 J_1^{\,2}(\mu R)} \tag{13}$$

(see Appendix C). The total helicity per unit length is now given by the sum of equations (9) and (13), $\tilde{K} = \tilde{K}_0 + \tilde{K}_1$. In accordance with the discusssion in § II*b*, we calculate the contribution of the $m = 1$ mode to the boundary pressure by averaging $[(B_\theta^{\,1})^2 + (B_z^{\,1})^2]^2/8\pi$ over θ. The pressure-balance condition then implies

$$R = \left\{\frac{(\mu R)^2}{2\pi p_e}\left(\frac{\Psi}{4\pi}\right)^2\left[1 + \frac{J_0^{\,2}(\mu R)}{J_1^{\,2}(\mu R)} + \frac{\epsilon^2}{2}\left(\frac{(\mu R + kR)^2}{Y^2} + \frac{(kR)^2 Y^2}{(\mu R - kR)^2}\right)\frac{J_0^{\,2}(Y)}{J_1^{\,2}(\mu R)}\right]\right\}^{1/4}, \tag{14}$$

which generalizes equation (10). We can similarly generalize the functions F_0, G_0, and H_0 by writing, in obvious notation, $\tilde{K}R/\Psi^2 = F_0(\mu R) + \epsilon^2 F_1(\mu R, kR)$; $p_e R^4/\Psi^2 = G_0(\mu R) + \epsilon^2 G_1(\mu R, kR)$; and by defining $H(\mu R, kR, \epsilon) \equiv p_e \Psi^6/\tilde{K}^4$. H can be reduced to a function of ϵ alone with the help of equation (12). Since we are interested in the lowest energy state, we only need to consider the minimum value of μR for which a solution of equation (12) exists (see Reiman 1980). This is found by a numerical calculation to be

$$(\mu R)_{\min} = 3.11\,, \tag{15a}$$

corresponding to

$$(kR)_{\min} = 1.25\,. \tag{15b}$$

Substituting these values into the defining relation for H, we obtain a quadratic equation for ϵ^2, with the value of H as a parameter. This equation yields positive solutions (corresponding to real values of ϵ) provided that H is *smaller* than a certain critical value given by

$$H_c \equiv \left(\frac{p_e \Psi^6}{\tilde{K}^4}\right)_c = 2.7 \times 10^3 . \tag{16}$$

If this condition is fulfilled, one can use the computed value of ϵ^2 in equation (14) to find R, and then, finally, to obtain $\tilde{W}$.

We have used these procedures to calculate $\tilde{W}$ as a function of p_e for given values of $\tilde{K}$ and Ψ. We display the result in a dimensionless form in Figure 2 by plotting $\tilde{W}\Psi^2/\tilde{K}^2$ versus log H. It is seen from this figure that, for sufficiently large values of p_e, only the $m = 0$ mode (*dashed curve*) exists. Along the $m = 0$ curve, μR increases with decreasing external pressure, reaching the value $(\mu R)_{\min}$ (eq. [15a]) at $H = H_c$ (eq. [16]). At that point, the mixed-mode state (*solid curve*) branches off. The specific value of p_e at which the bifurcation occurs depends on the magnitude of the conserved quantities Ψ and $\tilde{K}$: it is higher the lower the value of Ψ and the higher the value of $\tilde{K}$. Along the $(m = 0) + (m = 1)$ curve, the value of μR remains fixed at 3.11, whereas ϵ increases with decreasing p_e. It is evident from Figure 2 that, beyond the bifurcation point, the mixed-mode curve lies *below* the $m = 0$ curve. We have thus recovered Taylor's (1974, 1975) result (see also Reiman 1980) that, for values of μR in excess of 3.11, the mixed-mode configuration is energetically the favorable state. It is also easy to verify that all other modes have higher energies than the $m = 0$ mode, so that they need not be considered in this comparison. This follows from the fact that the condition $B_r(R) = 0$ for these modes is satisfied only for values of μR that exceed the asymptotic value of μR on the $m = 0$ curve, given by the first zero of the function J_1 (see eqs. [8] and [9]).

So far we have considered only "static" equilibria: Given the values of p_e, Ψ, and $\tilde{K}$, we have calculated the lowest-energy field configuration and the corresponding value of R. However, if the gas in the jet is able to maintain a minimal force-free configuration (with constant $\tilde{K}$ and Ψ) as it moves out, then one may interpret Figure 2 also as describing the dynamical evolution of the equilibrium state with distance along the jet. As is evident from this figure, the energy per unit length in the jet must in this case continuously decrease as the gas flows into regions of lower external pressure. One mechanism by which the gas loses energy is the $p_e dV_j$ work that it does on the external medium. When only the $m = 0$ mode is present, one can readily verify from equations (5) and (8)–(10) that this work is exactly in the amount that is required for remaining in the minimum-energy state. In the case of the mixed-mode state, however, the $p_e dV_j$ work is insufficient for maintaining the minimal field configuration, so energy must be dissipated at a rate per unit length of $\tilde{P}_m = -[(d\tilde{W}/dR) + 2\pi R p_e] v_j (dR/dz)$. Using equations (5), (8), (9), (13), and (15), we obtain $(d\tilde{W}/dR) = -(\tilde{W} + S)/R$. Substituting for p_e from equation (14), we then find that $\tilde{P}_m$ depends only on the $m = 1$ field component and is given by

$$\tilde{P}_m = 3.3 \times 10^{-3} B_1^2 v_j R \frac{dR}{dz} . \tag{17}$$

Although the pressure p_e is the independent physical parameter which varies along the jet, it is in general only the radius R which is directly measurable. In considering the observational implications of this model, it is thus more convenient to treat R as the independent variable. This is done in Figure 3, where we display the evolution of μR, ϵ, and p_e in the minimum-energy state for fixed

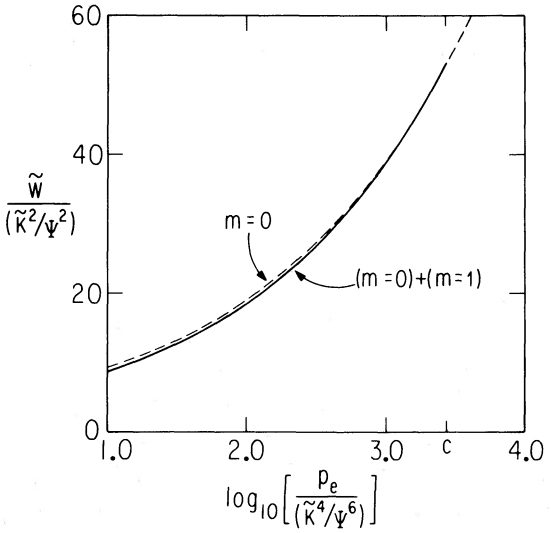

FIG. 2

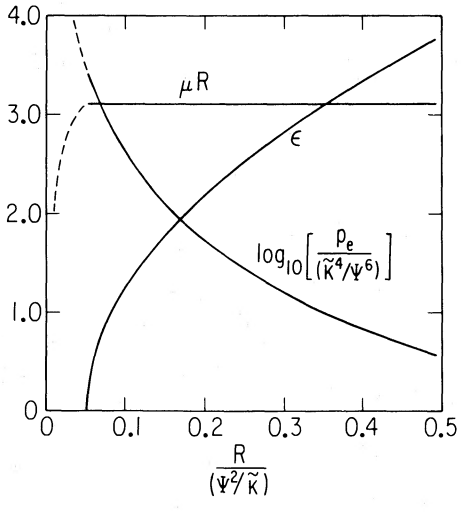

FIG. 3

FIG. 2.—The magnetic energy per unit length, $\tilde{W}$ (normalized by $\tilde{K}^2/\Psi^2$), as a function of the external pressure p_e (normalized by $\tilde{K}^4/\Psi^6$) for fixed values of $\tilde{K}$ (the magnetic helicity per unit length) and Ψ (the magnetic flux). The dashed and solid curves denote the pure $m = 0$ and the mixed-mode states, respectively. The letter c on the abscissa marks the bifurcation point (eq. [16]) where the mixed-mode curve branches off.

FIG. 3.—The variation of μR (where μ is the constant in the force-free field equation), ϵ (the ratio of the $m = 0$ and the $m = 1$ field amplitudes), and p_e (the boundary pressure) with radius R for the minimum-energy state at fixed specific helicity $\tilde{K}$ and flux Ψ. The dashed and solid portions of the curves correspond, respectively, to the pure $m = 0$ and the $(m = 0) + (m = 1)$ field configurations.

values of $\tilde{K}$ and Ψ. This figure shows explicitly the increase of μR in the pure $m = 0$ state, and of ϵ in the mixed-mode state, with decreasing p_e and increasing R. An *upper* limit on the rate of increase of μR with R is given by the small-R limit, $\mu R \propto R$ (cf. eq. [9]), whereas a *lower* limit on the variation of ϵ is given by the large-R limit, $\epsilon \propto R^{1/2}$ (cf. eq. [13]). The evolution of p_e with R reflects the behavior of the magnetic field amplitudes. In the limit $\epsilon \ll 1$ when the $m = 0$ mode dominates, B scales roughly as R^{-2}, as prescribed by the flux-conservation condition (eq. [7]). On the other hand, when $\epsilon \gg 1$ and the $m = 1$ mode dominates, the helicity-conservation condition (eq. [13]) implies $B \propto R^{3/2}$. We note that the radial scaling of B in the $\epsilon \gg 1$ limit is intermediate between the variations obtained by applying the flux-conservation condition separately to the longitudinal and to the transverse field components (see § I). This illustrates the fact that, if the jet is to remain in a minimum-energy state as well as conserve helicity during its expansion (see preceding paragraph), then the different field components cannot evolve independently.

d) Nonaxisymmetric Equilibria

The remarkable fact demonstrated by Figure 2 is that, for certain values of the external pressure and of the conserved parameters in the jet, the equilibrium configuration is likely to be *nonaxisymmetric*. This figure indicates, moreover, that even if the field convected by the outflowing gas initially has an axisymmetric structure, it may become nonaxisymmetric further out along the jet. In fact, as we noted in § IIc, if the field can continuously adjust to maintain a minimum-energy configuration while conserving helicity, then its behavior as the gas moves to regions of lower p_e may be inferred by tracing the descent of the $m = 0$ curve in this figure toward the bifurcation point ($\mu R = 3.11$). At that point, if the jet is dissipative, the field will switch over to the mixed-mode state. The $m = 0$ mode, however, is unstable to an $m = 1$ perturbation even within the framework of ideal MHD, albeit only for $\mu R > 3.18$ (Voslamber and Callebaut 1962). In the statistical model considered by Turner (1983*a*, *b*), one can associate the transition to a nonaxisymmetric configuration with the narrowing of the fluctuation spectrum about the mean $m = 0$ state down to a single $m = 1$ mode when the bifurcation point is approached. The fact that the nonaxisymmetric state contains no contributions from modes higher than $m = 1$ gives rise to its characteristic wavelength, $\lambda \approx 5R$ (eq. [15b]), which depends only on the value of the local radius but not on the amplitude of the nonaxisymmetric component.

The appearance of a nonaxisymmetric equilibrium is related to the fact that the system possesses more than one integral of motion (in this case, magnetic helicity *and* energy), and that these integrals exhibit selective decay (in this case, energy can be dissipated while helicity remains approximately conserved). This type of symmetry breaking is not unique to MHD and, in fact, occurs in other classical dynamical systems where these general conditions are fulfilled. Perhaps the most familiar example can be found in the theory of the equilibrium configurations of rotating fluid masses (e.g., Chandrasekhar 1969). In this case, if one considers the minimum-energy shape of a uniformly rotating, incompressible mass of fluid, one finds that for small angular velocities it is axisymmetric (a Maclaurin spheroid), but that as the angular velocity (and correspondingly the ellipticity e) increases, a bifurcation point is reached (at $e = 0.81$) where nonaxisymmetric configurations (Jacobi ellipsoids) become energetically favorable. The similarity with the MHD case is made all the more striking by the fact that, even in the absence of dissipation, the axisymmetric configurations become dynamically unstable somewhat beyond the bifurcation point (at $e = 0.95$). Here the integrals of motion are the angular momentum and the energy, and it is again the energy which is assumed to decay more rapidly. The preferentially dissipated quantity need not, however, be the energy. This is exemplified by two-dimensional Navier-Stokes turbulence, where energy cascades to longer wavelengths and is approximately conserved, whereas *enstrophy* (the volume integral of the vorticity squared) cascades to shorter wavelengths and is dissipated; this behavior again gives rise to nonaxisymmetric equilibria, a fact which has found applications in the study of oceans and planetary atmospheres (see Kraichnan and Montgomery 1980 for a review).

In view of the preceding examples, it seems reasonable to expect that nonaxisymmetric magnetic configurations would appear even in systems where the field had not relaxed to a force-free state, as long as the magnetic helicity remained conserved relative to the energy. Incomplete relaxation may occur if the system is only weakly dissipative, so that other global parameters in addition to the helicity are approximately conserved on the time scale of interest (Bhattacharjee, Dewar, and Monticello 1980). An alternative possibility (Turner and Christiansen 1981) is that, although the plasma is resistive, turbulent fluctuations lead to a continuous regeneration of the magnetic field (cf. De Young 1980). The hypothesis of incomplete relaxation was originally advanced to account for a number of observed features in reversed-field pinches which were inconsistent with the predictions of the force-free model. We recall from our discussion in § I, however, that pinch discharges also exhibit nonaxisymmetric configurations, which supports the conclusion that such behavior is not contingent on the field being force free. Although astrophysical jets may well be incompletely relaxed, this need not have a major effect on the basic structure of the magnetic field (cf. Turner and Christiansen 1981), and hence we continue to consider in the remainder of this paper only the simple, force-free model.

III. EMISSION PROPERTIES OF FORCE-FREE JETS

a) Calculation of the Stokes Parameters

As an application of our model, we consider in this section the expected distribution of the total and the polarized intensities from nonrelativistic, synchrotron-emitting jets with force-free magnetic field configurations. We assume that the emission is optically thin and that the jets are observed at large angles to their axes and are fully resolved. Since we are mainly interested in the effect of the magnetic field structure on the emission pattern, we model the spatial distribution N of the radiating particles very crudely by a Gaussian in the radial coordinate r, $N(r) = N_0 e^{-\kappa r^2/R^2}$, where $\kappa \ll 1$ corresponds to a nearly uniform distribution and $\kappa \gg 1$ represents strong concentration near the axis. We further suppose that, at each point, the emitting particles have an isotropic pitch-angle distribution and a power-law energy distribution corresponding to a spectral index α. Under these conditions, the total intensity received along a line of sight $\boldsymbol{e}_{x'}$ through the jet is given by

$$I(y', z') = C \int N(B_{y'}^2 + B_{z'}^2)^{(1+\alpha)/2} dx' , \tag{18}$$

where $\boldsymbol{e}_{y'}$ and $\boldsymbol{e}_{z'}$ are two orthogonal directions in the plane normal to the line of sight, and where the factor C incorporates all the constants in the problem (including the frequency of observation).

The polarized emission from the jet is best calculated with the help of the Stokes parameters Q and U (e.g., Gardner and Whiteoak 1966). In terms of these parameters, the degree of linear polarization is given by

$$P(y', z') = \frac{\sqrt{Q^2 + U^2}}{I}, \tag{19a}$$

whereas the position angle of the projected mean electric field vector is

$$\xi(y', z') = \frac{1}{2} \tan^{-1}\left(\frac{U}{Q}\right). \tag{19b}$$

Q and U are given, respectively, by

$$Q(y', z') = C \int N(B_{y'}^2 + B_{z'}^2)^{(1+\alpha)/2} p \cos 2\chi \, dx', \tag{20a}$$

and

$$U(y', z') = C \int N(B_{y'}^2 + B_{z'}^2)^{(1+\alpha)/2} p \sin 2\chi \, dx', \tag{20b}$$

where p is the intrinsic degree of polarization and where

$$\chi = \tan^{-1}\left(\frac{B_{y'}}{B_{z'}}\right). \tag{20c}$$

If the magnetic field is locally uniform, then p is given by

$$p = \frac{3\alpha + 3}{3\alpha + 5}; \tag{21}$$

however, in a turbulent plasma the degree of polarization could be substantially lower because of the random fluctuations about the mean field. We have not included in equation (20c) a term proportional to the rotation measure to the point of emission, which would have taken account of possible *depolarization* in the jet (e.g., Cioffi and Jones 1980). This omission is justified in the case of extended jets, where depolarization effects are generally small (see § III*b*).

Figures 4–6 illustrate some of the results of our calculations. In these figures we have set $\alpha = \kappa = 1$, but the results are qualitatively similar for $0.5 \lesssim \alpha \lesssim 1$ (the characteristic range of extended jets) and for $0 \lesssim \kappa \lesssim 2$. In Figure 4a we plot the

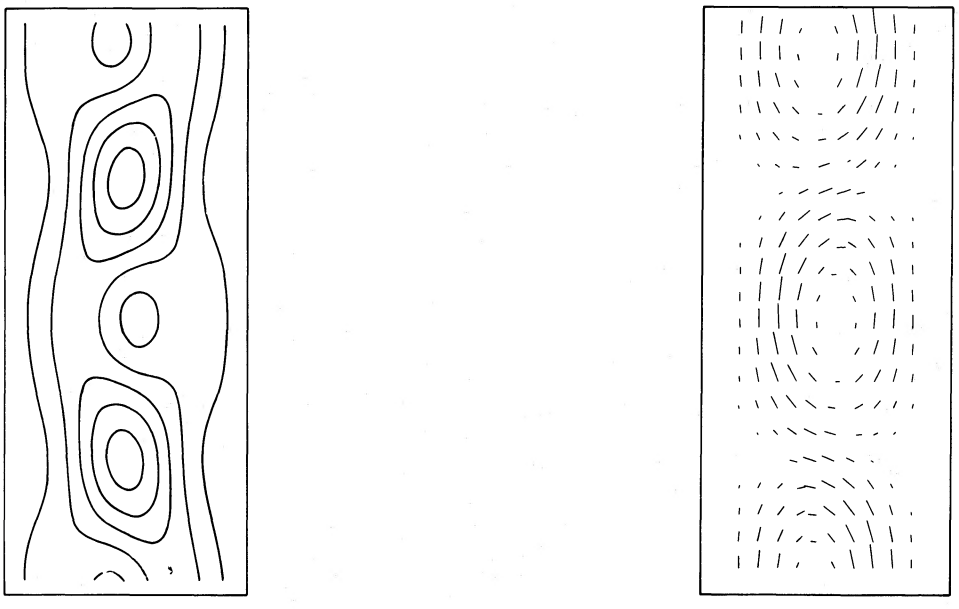

(*a*) (*b*)

FIG. 4.—The total-intensity contours (*a*) and projected magnetic field vectors (*b*) for a cylindrical, force-free jet with $\epsilon = 5$ that is observed at an angle $\delta = 90°$ to the axis. The synchrotron emissivity was calculated for $\alpha = \kappa = 1$ (see text for notation). In Fig. 4a, the contours represent $\frac{1}{6}, \frac{2}{6}, \ldots, \frac{5}{6}$ of the maximum intensity in the jet. In Fig. 4b, the length of each line segment is proportional to the magnitude of the local polarized intensity. The extent of the jet in these plots corresponds to one wavelength of the $m = 1$ mode.

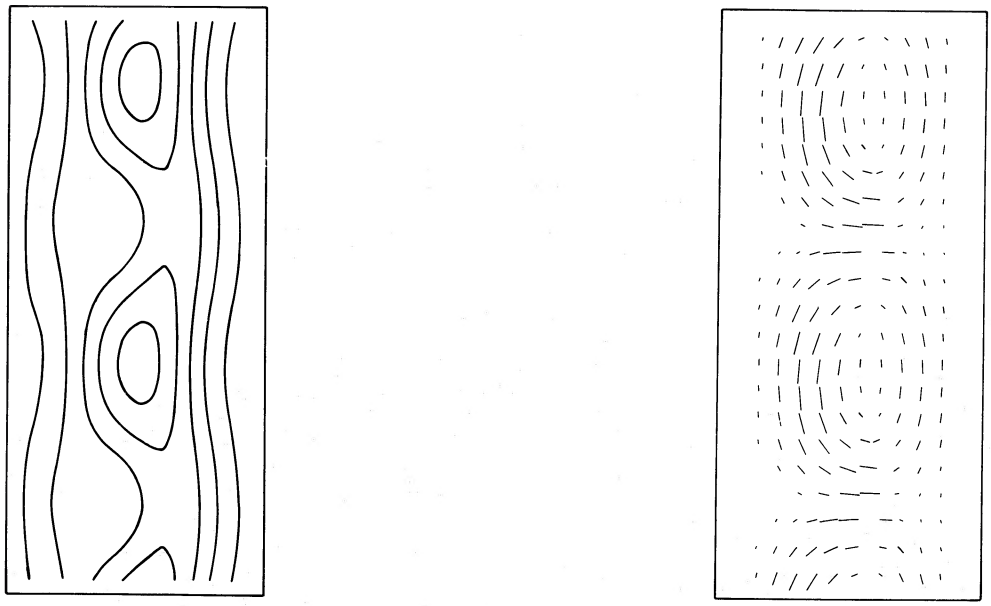

(*a*) (*b*)

FIG. 5.—Same as Fig. 4, except that $\epsilon \rightarrow \infty$ (pure $m = 1$ mode) and $\delta = 70°$

total-intensity contours for a mixture of the $m = 0$ and $m = 1$ modes (eqs. [6] and [11] with $\epsilon = 5$) in a jet observed at a right angle to the axis. Figure 4b shows the projected magnetic field vectors in this jet as they would have been inferred from polarization measurements after correcting for possible Faraday rotation effects along the line of sight to the jet. In this figure, the projected magnetic field vectors are represented by lines whose lengths are proportional to the polarized intensity $P \times I$ (see eq. [19a]), and whose orientations are obtained by adding 90° to the position angle ξ of the mean electric field (eq. [19b]). Figure 5 gives similar plots for a pure $m = 1$ field in a jet observed at an angle $\delta = 70°$ to the axis. In Figure 6 we display the variation of the total intensity I and of the degree of polarization P along the ridge line of the jet (defined as the locus of the peak intensity points along the jet) for the parameters of Figure 5. (The corresponding plots for the parameters of Fig. 4 are similar.) We now consider the implications of these results to the interpretation of resolved radio jets.

b) Application to NGC 6251

NGC 6251 is one of the best-studied examples of an extended, well-collimated jet. Recently, a high-resolution, multifrequency radio study by Perley, Bridle, and Willis (1984, hereafter PBW) has provided detailed information on the properties of the total and the polarized emission from this source. We have therefore chosen to concentrate on this jet in discussing the various observed features which can be interpreted by our model. Many of these features, however, have also been detected in other extended radio sources. We now list the main emission properties to which the results of § III*a* may be relevant; for a fuller description of the observations, we refer the reader to PBW or to the review article by Bridle and Perley (1984).

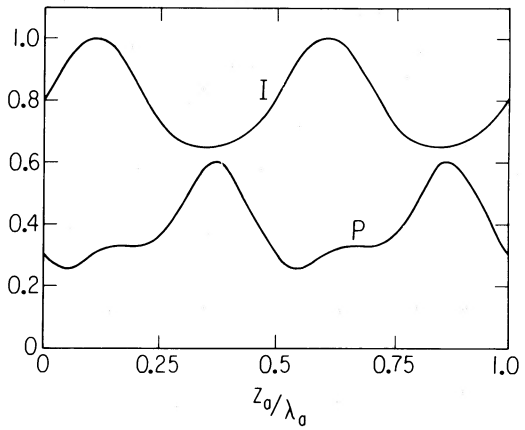

FIG. 6.—The variation of the total intensity I (normalized by its peak value) and of the degree of polarization P along the ridge line of the jet for the model considered in Fig. 5. The apparent distance z_a along the jet is measured in units of λ_a, the projected wavelength of the $m = 1$ mode.

i) *Transverse Oscillations of the Ridge Line*

Small oscillations of the ridge line about a mean position angle were found to occur at various locations along the jet (Fig. 7 in PBW). In the inner jet (at angular distances of 20″–40″ from the origin), these oscillations have a dominant wavelength of $\sim 9''$, whereas in the outer jet (between 120″ and 240″), the characteristic wavelength is $\sim 31''$. In the latter range, it has been determined that the oscillations result from changes in the symmetry of the transverse intensity profiles and do not involve the lower-intensity, outer radio contours. (The transverse resolution in the inner jet was not good enough to permit a similar determination there.) Beyond $\sim 240''$, the jet is dominated by a long-wavelength ($\sim 143''$) oscillation which involves both the outer isophotes and the ridge line. As was discussed by PBW, the 143″ oscillation could be attributed either to a helical Kelvin-Helmholtz instability or to a precession of the central source, but neither one of these mechanisms is likely to account for the shorter-wavelength oscillations. In particular, for the relatively high Mach numbers ($M \sim 10$) and the low internal-to-external density ratios ($\eta < 1$) estimated for this jet by PBW, the wavelength of the fastest-growing helical Kelvin-Helmholtz mode is predicted to be much larger than the radius R of the jet (cf. Ferrari, Trussoni, and Zaninetti 1983). In contrast, the actual oscillation wavelengths in the inner and outer regions of the jet are only $\sim 4.7R$ and $\sim 5.6R$, respectively (where R is estimated as one-half the average FWHM in the given region).

The appearance of transverse oscillations is, however, a natural consequence of the presence of an $m = 1$ mode in the equilibrium configuration of a force-free jet. The oscillations in this case can arise in one of two ways, illustrated in Figures 4a and 5a, respectively. The first possibility (Fig. 4a) corresponds to the magnetic field containing comparable contributions from the $m = 0$ and $m = 1$ modes (i.e., $\epsilon \sim 1$). To understand the origin of this effect, assume that the jet is seen at a right angle to its axis, and consider the plane containing both the axis and the line of sight to the observer. It is clear from equation (11) and Figure 1 that, for any given point in the jet on one side of this plane, there exists a point on the other side of the plane (obtained by reflection through the axis) such that the field components $B_\theta{}^1$ and $B_z{}^1$ at the two points are equal in magnitude but opposite in sign. On the other hand, the components $B_\theta{}^0$ and $B_z{}^0$ (eq. [6]) have the same magnitude *and* the same sign at both points. Thus, the contributions from the two modes will add with opposite signs on the two sides of the midplane, resulting in a higher net field on one side and a shift of the ridge line away from the axis. Because of the phase dependence of the $m = 1$ mode, the ridge line will oscillate from one side of the axis to the other with the wavelength $\lambda \approx 5R$ of this mode. This value of λ is in close agreement with the average values inferred for the short-wavelength oscillations in both the inner and the outer regions of the NGC 6251 jet. (Note that the FWHM increases only by a factor ~ 5 between these two regions [Fig. 10 in PBW], so that if ϵ were of order unity in the inner jet, it would remain so also in the outer jet; cf. Fig. 3.) As can be seen from Figure 4a, this effect does not involve the outer intensity contours, again in agreement with the observations. This, however, is mainly a result of the fact that $B_z{}^0$ vanishes at $r = 0.77R$ (cf. eqs. [6] and [15a]), and hence would not apply if the emission from the vicinity of the boundary were too weak to be detected. (The latter situation might arise if the radiating-particle distribution N were highly concentrated near the axis [$\kappa \gg 1$].)

The above mechanism applies also to jets seen at an angle $\delta < 90°$, so long as ϵ remains of order unity. When $\delta \neq 90°$, there is, however, another effect which comes into play and which could lead to apparent transverse oscillations of the ridge line even in jets with $\epsilon \gg 1$ (see Fig. 5a). This second possibility of producing oscillations arises from the magnetic field geometry in the $m = 1$ mode, which is essentially that of two twisted, oppositely directed flux tubes wrapped around each other (see Fig. 1). When this configuration is viewed at an oblique angle ($\delta < 90°$), it gives rise to an apparent transverse oscillation of the peak magnitude of the magnetic field component normal to the line of sight and, hence, to an oscillation of the synchrotron-emission ridge line (see eq. [18]). In this case, however, the ridge line does not cross the jet axis, and the oscillation wavelength corresponds to a distance of only $\lambda/2$ along the jet (the apparent wavelength is further reduced by a factor of $\cos \delta$). The pure $m = 1$ effect is therefore distinguishable, in principle, from the mixed-mode mechanism. In the case of the NGC 6251 jet, it is the mixed-mode interpretation which seems to be favored by the observations. However, because of the scatter in the individual data points for the FWHM (Figs. 10 and 11 in PBW) and the apparent discrepancy between them and the measured isophotal widths (§ IV*d* in PBW), and also because of the ambiguity in the position of the center line of the jet, one cannot yet rule out the possibility that the oscillations are produced by a pure $m = 1$ mode. In either case, however, one can conclude that the inclination angle δ is not smaller than $\sim \tan^{-1}(4R/\lambda) \approx 40°$, for otherwise the line of sight would penetrate more than $\sim \lambda/2$ along the jet, and the effects discussed above would be washed out. Furthermore, from either one of these interpretations it follows that, after the intensity profiles in the inner jet of this source are fully resolved with a high dynamical range, it should again be found that the transverse oscillations involve mainly the inner isophotes.

ii) *Oscillations of the Jet's Width and the Appearance of Emission Knots*

As in most other extended jets, the radio maps of NGC 6251 show a knotty substructure (Fig. 3 in PBW). This substructure manifests itself in the form of oscillations of the total intensity along the ridge line of the jet, which appear to anticorrelate with oscillations of the FWHM (Fig. 10 in PBW). Both of these features may be attributed to the pinching ($m = 0$) Kelvin-Helmholtz instability (e.g., Hardee 1982; Cohn 1983). This interpretation is consistent with the measured wavelengths of these two types of oscillation and with their apparent anticorrelation, but, as has already been emphasized by PBW, it does not explain why they occur on the same scale as the transverse oscillations of the ridge line. All these effects, however, can be given a unified interpretation in the context of our equilibrium model. As can be seen from Figures 4a and 5a, the transverse oscillations calculated from this model are accompanied by oscillations of the isophotal width. The latter, in turn, are anticorrelated with the oscillations of the peak intensity along the jet which trace the distribution of bright emission knots (see Fig. 6). We emphasize that, in contrast to the previous interpretation, in this picture the changes in the measured width and the appearance of emission knots are simply by-products of the magnetic field structure in the jet and do not involve any compression of the flow. As in the case of the transverse oscillations, these effects are washed out when the inclination angle becomes small ($\delta \lesssim 40°$). We note that the oscillations of the isophotal width in our model are reflected also in the behavior of the FWHM, so long as the latter is a well-defined quantity. The FWHM is not well defined when $\delta \approx 90°$, $\epsilon \gg 1$, and $\kappa \lesssim 1$, since in that case some of the transverse intensity profiles are double-peaked. However, in light of our earlier discussion, this combination of parameters is not expected to occur in regions which exhibit measurable transverse oscillations of the ridge line.

iii) *Projected Magnetic Field Configuration*

One of the most striking results of the polarization measurements in NGC 6251 is the systematic appearance of projected magnetic field vectors that are oblique with respect to the jet's axis and that, in a number of locations, show an oscillatory variation in orientation with distance along the jet (Figs. 22 and 23 in PBW). This behavior is readily accounted for in our model (see Figs. 4b and 5b), where it is a direct consequence of the nonaxisymmetric structure of the field (§ II*d*). In fact, the ability to account for oblique magnetic field configurations is a distinguishing property of this model, since axisymmetric models can only give rise to projected field vectors that point either along or at a right angle to the axis. Our model, however, may also account for other aspects of the inferred magnetic field distribution. In particular, it is possible to attribute the transition from a predominantly parallel to a predominantly perpendicular projected field along the axis of the jet that is observed in NGC 6251 (as well as in most other jets associated with a relatively weak central source) to the increase of ϵ with decreasing external pressure for fixed Ψ and $\tilde{K}$ (see Fig. 3). This is a consequence of the fact that the ratio $B_\theta{}^0/B_z{}^0$ is small, whereas the ratio $B_\theta{}^1/B_z{}^1$ is large, in the region $r \ll R$ where most of the observed emission from the projected center of the jet originates (see eqs. [6] and [11]). We find that a significant perpendicular component appears in our model for ϵ of the order of a few (the precise value depending on the concentration parameter κ and the inclination angle δ), but that the projected field may still be nearly parallel to the axis even when the contribution from the $m = 1$ mode is already large enough to cause apparent transverse oscillations and a knotty substructure. (These latter features can thus be accounted for even when they occur in regions where the observed field is still predominantly parallel, as in the inner jet of NGC 6251.) The fact that, in our model, the $m = 1$ mode is responsible for both the departure of the field geometry from axisymmetry and the appearance of knots provides a natural explanation of the observed tendency of oblique-field regions to be associated with bright emission knots. (See § VII*a* in PBW for an alternative interpretation in terms of oblique shocks.) Furthermore, since for large inclination angles the main contribution to the synchrotron emission from the edges of the jet comes from the z-component of the magnetic field (as $B_r(R) = 0$, and $B_\theta(R)$ lies approximately along the line of sight), it follows that the observed persistence of a parallel-field configuration at the periphery of the jet, even in regions where the field near the center is predominantly transverse, can be accounted for without having to invoke surface shear (cf. Baan 1980). This feature, in fact, is a general property of helical field models (Laing 1981). We note, however, that the simple, force-free configurations that we have calculated do not reproduce the extended regions of predominantly transverse fields that are detected near the axis of the outer jet in NGC 6251 as well as in a number of other jets (see Bridle and Perley 1984). Possible explanations of this behavior could be that only a fraction of the emitting volume in these jets is magnetic-pressure dominated, or else that these jets are incompletely relaxed (see § II*d*).

iv) *Oscillations of the Degree of Polarization*

Another parameter which was found to display periodic oscillations along the ridge line of the jet is the degree of linear polarization (Fig. 16 in PBW). As is seen from Figure 6, this feature, too, is predicted by our model. In this figure, the maxima of P are correlated with the minima of the total intensity I. In addition, our calculations indicate that the degree of polarization in this model is generally higher near the edges of the jet than at the center. Both of these properties are in agreement with the observational findings in the inner jet and in some portions of the outer jet of NGC 6251 (see Figs. 10, 15, and 16 in PBW). However, there are also some regions in the outer jet where the opposite behavior is found, namely, the peak value of P on the ridge line coincides with the local maximum of I, or else P is larger at the center than near the edges. One possible explanation of this complex behavior is the presence of a fluctuating magnetic field component in the jet. The presence of such a component is also indicated by the need to reconcile the relatively high values of P that are predicted in this model (see Fig. 6) with the significantly lower values that are actually measured (see § VII*c* in PBW). The most likely origin of such a fluctuating field is internal turbulence which, as we pointed out in § II*a*, may already be an ingredient of the general equilibrium model.

v) *Distribution of the Faraday Rotation Measure*

The Faraday rotation-measure distribution in the inner jet is characterized by strong gradients both along and across the jet (Figs. 20, 21, and 27 in PBW). These gradients most likely arise from changes in the line-of-sight component of the local magnetic field (see § VII*b* in PBW) and, therefore, can be regarded as another direct manifestation of a nonaxisymmetric field distribution. It was found that reversals in the sign of the RM gradient along the jet, and the strongest RM gradients across the jet, both occur on a scale *along* the jet which is of the order of the scale of the aforementioned transverse oscillations of the ridge line (as well as of the oscillations of I and P along the ridge line). It is thus plausible to attribute the RM gradients to the same general field distribution which gives rise to the apparent oscillations of the total and the polarized intensities. However, as was pointed out by PBW (and as we verified explicitly with our model), it is unlikely that much of the Faraday rotation originates in the emitting material itself, since in that case one would expect to detect substantial depolarization effects, whereas the observed degree of polarization is nearly independent of frequency. PBW interpreted the data as pointing to a magnetized sheath around the jet, and they noted that the external magnetic loops could help confine the outflow if the jet carried a net axial current. This possibility is consistent with the identification of the sheath with a "cocoon" of jet material that is being continuously supplied at the head of the jet (cf. Achterberg, Blandford, and Goldreich 1983). In that case, the external field configuration might again correspond to the minimum-energy state of a magnetically dominated plasma with a conserved magnetic helicity. Thus, the field outside the jet might also be force free, and if the "cocoon" material moved supersonically with respect to the confining ambient medium (which should be the case for highly supersonic, relatively low-density jets; see Norman *et al.* 1982), then the approximation of locally cylindrical boundaries would continue to apply (see Appendix B). Under these conditions, it may, in principle, be possible to generalize the solution presented in § II*c* to include both the jet and the sheath. However, since there are now *two* boundary conditions to be satisfied ($B_r = 0$ at the boundary of the jet *and* at the surface of the sheath), and since the Chandrasekhar-Kendall modes in the sheath contain both Bessel and Neumann functions (cf. eq. [4]), this problem is formally much more involved and we do not pursue it further here.

In the model that we have presented, it is possible to interpret the various nonaxisymmetric and oscillatory features that are

detected in NGC 6251 in terms of the $m = 1$ mode alone. It is, however, also possible that the $m = 0$ mode still contributes substantially to the field, and we suggested that this could in principle be tested observationally by an analysis of the transverse oscillations of the ridge line. If the $m = 0$ contribution were large, then one would be faced with the usual problem of a magnetic flux much larger than what could reasonably be expected to exist near the origin of the jet (e.g., Rees, Begelman, and Blandford 1981). One possible resolution of this problem could be that the jet undergoes more than one subsonic-to-supersonic nozzle transition on the way out from the galactic nucleus, and that each such step in the cascade involves substantial entrainment of mass and magnetic flux from the surrounding medium (e.g., Henriksen, Bridle, and Chan 1982). Even in the latter interpretation, however, the inferred field strength in the supersonic portions of the jet is required for self-consistency to be low enough for the Alfvén speed to remain smaller than the velocity of the jet. In the case of NGC 6251, we may obtain a *lower* limit on the Alfvén speed in the extended jet by combining the equipartition field B_{eq} (Table 2 in PBW) with the upper limit on the thermal electron density n_e inferred from the depolarization measurements (§ VII*e* in PBW). For the inner jet ($B_{eq} \approx 3 \times 10^{-5}$ gauss, $n_e < 4 \times 10^{-3}$ cm^{-3}), this yields an Alfvén speed $\gtrsim 9 \times 10^7$ cm s^{-1}, which is about an order of magnitude smaller than the estimated lower limit on the jet velocity (§ VII*f* in PBW). Although these estimates are rather uncertain, they nevertheless appear to be consistent with the presence of a nonnegligible $m = 0$ component in the large-scale outflow from this source.

Finally, we consider the question of whether the observed synchrotron emission from this jet could represent the energy that is being dissipated in the process of maintaining the lowest-energy magnetic field configuration. To be specific, we assume that the field everywhere obeys equation (3), and that the values of Ψ and $\tilde{K}$ are constant along the jet. As we discussed in § II*c*, no energy needs to be dissipated under these circumstances so long as the field is in the pure $m = 0$ state, a conclusion which is consistent with the fact that nonaxisymmetric phenomena are detected throughout the entire length of the observed (large-scale) jet. For the mixed-mode state, we found that energy must be dissipated at a rate per unit length given by equation (17). We may obtain a lower limit on the mean value of this power in the inner ($< 120''$) jet by substituting for B_1 the average equipartition value, $B_{eq} \approx 20$ microgauss, and estimating the mean values of $R (\approx 3 \times 10^{21}$ cm) and $dR/dz (\approx 0.05)$ from the FWHM data (Table 2 in PBW). Together with the lower limit on v_j given by PBW ($\approx 8 \times 10^8$ cm s^{-1}), these estimates yield $\tilde{P}_m \approx 2 \times 10^{17}$ ergs s^{-1} cm^{-1}. This value is comparable to the mean radio luminosity per unit length measured in this region (Fig. 13 in PBW), which supports the hypothesis that the dissipated magnetic energy is carried away by nonthermal radiation. The radio luminosity, however, is again just a lower limit on the total synchrotron power emitted in the jet. It is, therefore, conceivable that, while $\tilde{P}_m$ and the synchrotron luminosity per unit length may indeed be comparable, their actual values are substantially higher than the lower limits estimated above. If this is in fact the case, then the evolution of the radio luminosity per unit length along the jet need not be correlated with that of $\tilde{P}_m$. This could resolve the apparent discrepancy between the relatively slow decrease of the mean radio luminosity along the inner jet (Fig. 13 in PBW) and the much faster decline expected on the basis of equation (17).

The possibility that synchrotron radiation is the main dissipation mechanism in jets has previously been suggested in the context of turbulent jet models. One plausible scenario (e.g., Henriksen, Bridle, and Chan 1982; Bicknell and Melrose 1982) is that the dissipation is mediated by MHD waves which accelerate the synchrotron-radiating particles by the Fermi process. In those models, the source of energy for the turbulence was assumed to be the relative motion between the jet and the confining external medium which gave rise to a Kelvin-Helmholtz instability. As we noted in § II*a*, the equilibrium model considered in this paper has a natural interpretation in terms of MHD turbulence, and this may well be maintained by shear. However, in view of the discussion in the preceding paragraph (and the experience from reversed-field pinch experiments; see § I), it is conceivable that the main source of power for the turbulence is the magnetic energy liberated in the internal field-redistribution process. (We note in this connection that the longitudinal field components in the jet would tend to stabilize the Kelvin-Helmholtz modes for M_A not much greater than 1; e.g., Ferrari, Trussoni, and Zaninetti 1983.) It is worth pointing out, though, that the conversion of magnetic energy into synchrotron radiation need not necessarily be mediated by turbulence. An alternative possibility is that the radiating particles are accelerated directly by the DC electric fields induced during magnetic field reconnection. One mechanism that is likely to play an important role in this process is the resistive tearing-mode instability, which is also believed to contribute to efficient particle acceleration in solar flares (e.g., Heyvaerts 1981). The possible relevance of this instability to energy dissipation in force-free jets is indicated by the fact that the $m = 0$ field component becomes unstable to resistive tearing precisely at the branching point ($\mu R = 3.11$) of the mixed-mode state (Gibson and Whiteman 1968). The continued expansion of the jet beyond that point (as a result of the decline in the external pressure) would, in the absence of dissipation, increase μR above 3.11 (see Fig. 3) and thereby trigger the instability. The subsequent development of the instability could then conceivably restore the field to the minimum-energy configuration.

IV. CONCLUSIONS

In this paper we have presented a new model of magnetized, supersonic jets. We considered jets which are magnetic-pressure dominated, and which are therefore likely to settle into a *force-free* configuration ($\nabla \times \boldsymbol{B} = \mu \boldsymbol{B}$). We argued that the *magnetic helicity* (eq. [1] and Appendix A), which is a measure of the topological linkage of the field lines, is a key parameter which can play a central role in determining the magnetic field structure in such jets. This parameter is an integral of motion for a perfectly conducting jet, and it should also remain approximately conserved in a dissipative jet with a high magntic Reynolds number. This property can be formulated as a variational principle (§ II*a*) and implies that the coefficient μ in the magnetic field equation is locally a constant.

In considering the solutions of the field equation, we noted that the supersonic relative motion endows the ambient medium with an effective rigidity which limits the size of surface ripples (Appendix B). The boundary nevertheless remains free, in the sense that the mean radius R is determined by the magnitude of the confining external pressure. We showed that, under these conditions, the *minimum-energy* magnetic field configuration is, in general, a superposition of only *two* modes (Fig. 1): an axisymmetric ($m = 0$) mode (eq. [6]) which carries the net flux and axial current in the jet, and a helical ($m = 1$) mode (eq. [11]) of wavelength $\lambda \approx 5R$. For given values of the conserved flux and helicity, only the $m = 0$ mode is present at high external pressures (Fig. 2). As the confining

pressure decreases, both R and μR increase (Fig. 3) until, when μR reaches 3.11, the $m = 1$ mode becomes energetically favorable. Beyond the bifurcation point (eq. [16]), lower values of external pressure correspond to higher values of ϵ, the $m = 1$ to $m = 0$ amplitude ratio, but the value of μR remains fixed. For given values of magnetic helicity and external pressure, ϵ is larger the smaller the flux carried in the jet. In contrast to the axisymmetric, self-similar solutions considered for thermal-pressure-dominated jets (Chan and Henriksen 1980), the minimum-energy, force-free configurations considered in this paper are, in general, neither axisymmetric (except in the limit $\epsilon \ll 1$) nor self-similar (except in the limit $\epsilon \gg 1$). We pointed out (§ I) that nonaxisymmetric field configurations of this type have been observed in laboratory experiments on reversed-field pinches under conditions that are basically analogous to those that we have postulated for extragalactic jets. We also noted (§ II*d*) that the appearance of minimum-energy states that are nonaxisymmetric seems to be a general property of dynamical systems with more than one integral of motion (in this case, magnetic energy and helicity) which decay at different rates.

We applied our model to the interpretation of the total and the polarized synchrotron emission properties of resolved jets that are observed at a large angle to the axis (§ III). We found that it can account in a natural and unifying way for many of the key features of extended jets like NGC 6251, including the transverse oscillations of the ridge line (Figs. 4a and 5a), the oscillations of the jet's width and the appearance of emission knots, the oblique orientations of the projected magnetic field vectors with respect to the jet axis (Figs. 4b and 5b), the oscillations of the degree of linear polarization along the ridge line (Fig. 6), and the distribution of the Faraday rotation measure. All of these periodic phenomena are attributed in this model to the basic oscillation of the $m = 1$ mode and have a wavelength along the jet of either λ or $\lambda/2$. The model predicts that the apparent transverse oscillations should involve mainly the inner isophotes of the jet (which is in contrast with the behavior expected in the Kelvin-Helmholtz interpretation), and that the oscillations of the total intensity and of the degree of linear polarization along the ridge line should be anticorrelated. The model also implies a method of testing whether an apparently nonaxisymmetric jet carries a substantial amount of flux (which would correspond to ϵ being of order unity). For, if that were the case, then the transverse oscillations of the ridge line would be symmetric about the center line of the jet (as defined by the outer isophotes) and would occur at roughly twice the wavelength of the intensity oscillations along the ridge line. By contrast, if the amount of flux were small (corresponding to $\epsilon \gg 1$), then the transverse oscillations would occur only on one side of the axis, and their wavelength would be comparable to that of the intensity oscillations. The resolution of this question may have important implications for the origin of large-scale jets (§ IIIb). Despite the apparent successes of this model, we emphasize that it nevertheless is not in complete agreement with the observations. In particular, it does not in its present form reproduce the extended regions of predominantly transverse fields that are observed near the axis of a number of jets at large distances from the origin. This discrepancy could conceivably be attributed to the fact that these jets have not entirely settled into the minimum-energy, force-free configuration.

We have briefly explored the possibility that synchrotron radiation is the main dissipation mechanism which enables the magnetic fields in the jet to achieve the minimum-energy configuration. In particular, we considered whether the observed synchrotron emission could represent the magnetic energy that had to be dissipated during the expansion of a force-free jet to keep it in the lowest energy state. We found that the amount of energy dissipated in this fashion depends on the amplitude of the $m = 1$ mode (eq. [17]) and that it vanishes for $\epsilon = 0$, since the work done against the external pressure is then exactly in the amount of the required energy loss. In the case of the NGC 6251 jet, it turned out that the lower limit on the mean dissipation rate estimated on the basis of this model is comparable to the observed radio luminosity. This led us to speculate that, at least in some jets, the energy dissipated in the field-redistribution process might be the main source of energy for the synchrotron emission. One could then attribute the gaps in radio emission that are observed near the origins of certain extended jets to the fact that the ambient pressure in those regions is relatively high, so that $\epsilon \approx 0$ (see Fig. 3) and the dissipation is negligible. According to this interpretation, all observable force-free jets are necessarily nonaxisymmetric. (It is, however, conceivable that the absence of magnetic energy dissipation in the gaps is mainly the result of a relatively high thermal-to-magnetic pressure ratio in the innermost regions of the jet.) In addition, we pointed out the possible role of the resistive tearing-mode instability in the field-reconnection and particle-acceleration processes, and commented on its likely importance also in solar flares. In fact, there appears to be a basic similarity between the energy dissipation mechanisms envisioned in this model and those which are thought to operate in solar flares (and, more generally, in the heating of the solar corona). In both instances, it is the release of magnetic energy stored in twisted and braided magnetic field lines which is the immediate source of power for the emitted radiation, and in both cases the minimum accessible energy state may correspond to a force-free field with a constant μ (see Norman and Heyvaerts 1983). This suggests that studies of the magnetic activity in the solar corona could provide useful clues for a more detailed model of magnetic energy dissipation in jets.

We gratefully acknowledge valuable conversations with R. Blandford, G. Lake, and E. Parker. We also thank A. Bridle, G. Field, R. Henriksen, C. McKee, R. Perley, L. Turner, and P. Vandervoort for helpful comments, and B. Fryxell for assistance with the numerical computations. This research was supported in part by NASA grant NGL 14-001-001.

APPENDIX A

CONSERVATION OF MAGNETIC HELICITY

In discussing the conservation of the magnetic helicity K (eq. [1]) in the jet, it is convenient to assume that the jet forms a closed loop, or, equivalently, that the two ends of the jet can be identified. This identification is based on the hypothesis that the conditions at the origin of the jet—particularly the rates of injection of mass and magnetic helicity—are time invariant, and it enables us to avoid having to include source and sink terms for the flow. The boundary of the jet is defined by the outermost streamlines of the flow, and it is assumed to constitute a magnetic surface (i.e., $\boldsymbol{B}_s \cdot \boldsymbol{s} = 0$, where $\boldsymbol{B}_s$ is the surface magnetic field and $\boldsymbol{s}$ is the local normal

to the boundary). We further suppose that both the jet material and the external medium which confines it can be treated as perfect conductors. If the jet can be approximated by a cylinder of radius R, these conditions imply

$$B_r(R) = 0\,, \qquad A_\theta(R) = \frac{\Psi}{2\pi R}\,, \qquad A_z(R) = 0\,, \tag{A1}$$

where $\boldsymbol{A}$ is the vector potential and Ψ is the net axial flux in the jet. The radius R is determined by the value of the external pressure p_e (see § II*b*). We can imagine a hypothetical homogeneous jet which is confined by a uniform pressure, so that the value of R is constant. Under these conditions, it is meaningful to define the helicity per unit length $\tilde{K}$ and treat it as a constant of the flow. If the pressure p_e is allowed to vary to a new (uniform) value, then there will be a corresponding change in the radius R, but the total magnetic helicity K (and hence also $\tilde{K}$) will be conserved. This conclusion follows directly from the assumption of perfect conductivity and the condition $\boldsymbol{B}_s \cdot \boldsymbol{s} = 0$, and it is independent of the choice of gauge for $\boldsymbol{A}$ (e.g., Moffatt 1978, pp. 44–45). If we now substitute for the Eulerian (temporal) variations of p_e and R in the hypothetical jet the Lagrangian (convective) variations experienced by a real, super-Alfvénic jet, then it is clear that the conclusion regarding the conservation of $\tilde{K}$ will not change. As an illustration of the generality of this result, consider the magnetic helicity of a fluid element that is confined between two transverse cross sections of a cylindrical, thermal-pressure-dominated jet. The jet is assumed to flow supersonically, so the length L of the element remains constant even though its radius R may change. We suppose that the longitudinal and the transverse field components in the jet evolve according to the flux-freezing constraints (see § I) while maintaining an axisymmetric, radially self-similar configuration. Specifically,

$$\frac{B_\theta}{B_0} = \Theta(u)\,\frac{R_0}{R}\,, \qquad \frac{B_z}{B_0} = Z(u)\left(\frac{R_0}{R}\right)^2\,, \tag{A2}$$

where $u = r/R$, and where B_0 and R_0 are constants (cf. Bicknell and Henriksen 1980). The corresponding vector-potential components which satisfy the boundary conditions (A1) are

$$A_\theta = \frac{{R_0}^2}{R}\,\frac{B_0}{u}\int_0^u u' Z(u')du'\,, \qquad A_z = B_0 R_0\left[\int_0^u \Theta(u')du' - \int_0^1 \Theta(u')du'\right]. \tag{A3}$$

Hence, the total magnetic helicity of this element is

$$K = \frac{{B_0}^2 {R_0}^3 L}{4}\left[\int_0^1 \left\{\frac{\Theta(u)}{u}\int_0^u u' Z(u')du' + Z(u)\left[\int_0^u \Theta(u')du' - \int_0^1 \Theta(u')du'\right]\right\} u du\right], \tag{A4}$$

which is manifestly a constant, independent of R.

APPENDIX B

A LIMIT ON THE SURFACE RIPPLES IN A SUPERSONIC JET

We wish to substantiate the claim, made in § II*b*, that the magnitude ΔR of the ripples on the surface of a supersonic jet with mean radius R and Mach number (with respect to the external medium) $M_e \gg 1$ does not exceed $\sim R/M_e$. These ripples will form as a result of the periodic pressure variations induced by the $m > 0$, $k > 0$ modes of equation (4) that contribute to the total magnetic field at the surface. As long as $\Delta R \ll R$, the pressure associated with any one such mode varies on the surface essentially as $\cos^2(m\theta + kz)$, with a wavelength λ of at most a few times R ($\lambda \approx 5R$ for the $m = 1$ mode). The largest possible contribution to ΔR from the given mode can be estimated by assuming that it contributes most of the magnetic pressure at the boundary, so that its pressure amplitude is of the order of the external pressure p_e. The surface ripples induced by this mode travel through the ambient medium with the speed of the jet. To accommodate the passage of these ripples, the ambient gas can move sideways at most with its own speed of sound $v_{se} \approx (p_e/\rho_e)^{1/2}$. The maximum amplitude of the ripples is thus given by equating $\Delta R/v_{se}$ with the transit time of each ripple, $\lambda/v_j \lesssim R/v_j$. Larger-amplitude ripples will induce shocks in the ambient gas and will be damped, hence $\Delta R \lesssim R/M_e$. Another way of stating this result is that supersonically moving ripples can protrude into the ambient medium at most at the Mach angle $\sin^{-1}(1/M_e) \approx 1/M_e$. This behavior has been observed in numerical simulations of the nonlinear behavior of a supersonic Kelvin-Helmholtz instability (e.g., Tajima and Leboeuf 1980).

We can check the self-consistency of this result by considering the same situation in the rest frame of the jet. In this frame, the excess pressure associated with the given mode induces at the boundary a force (per unit volume) of magnitude $\sim p_e/\Delta R$, which must be balanced by the centrifugal force per unit volume $\sim(\rho_e {v_j}^2 \Delta R/\lambda^2) \gtrsim (\rho_e {v_j}^2 \Delta R/R^2)$ that is exerted by the external gas as it moves around the ripple. This implies $\Delta R \lesssim R/M_e$, in accordance with the previous derivation.

APPENDIX C

EVALUATION OF $\tilde{K}_1$

By constructing the vector potential corresponding to the $m = 1$ field components (eq. [11]) and imposing the boundary conditions given by equation (A1), one can readily verify that $(\boldsymbol{A} \times \boldsymbol{B})_r|_{r=R} \equiv 0$, so that $\int_{\Sigma_j} \boldsymbol{A} \times \boldsymbol{B} \cdot d\boldsymbol{\Sigma}_j = 0$ (see eq. [5]). Hence,

$$\tilde{K}^1 = \frac{1}{\mu}\tilde{W}^1 = \frac{1}{8\pi\mu}\int_0^R \int_0^{2\pi} [(B_r{}^1)^2 + (B_\theta{}^1)^2 + (B_z{}^1)^2] r d\theta dr \, . \tag{C1}$$

Integrating over θ and rearranging, we obtain

$$\tilde{K}^1 = \frac{\epsilon^2 B_0{}^2 R^3}{8(\mu R)Y^4}\{[(\mu R)^2 + (kR)^2]I_1 + Y^2 I_2 - (\mu R - kR)^2 I_3 + 2(\mu R - kR)^2 I_4\} \, , \tag{C2}$$

where

$$Y \equiv [(\mu R)^2 - (kR)^2]^{1/2} \, , \qquad I_1 \equiv \int_0^Y J_0{}^2(y) y dy \, , \qquad I_2 \equiv \int_0^Y J_1{}^2(y) y dy \, , \qquad I_3 \equiv \int_0^Y J_0(y) J_1(y) dy \, , \qquad \text{and} \qquad I_4 \equiv \int_0^Y \frac{J_1{}^2(y)}{y} dy \, .$$

I_1 and I_2 are the standard Bessel-function integrals (e.g., Gradshteyn and Ryzhik 1965, p. 634):

$$I_1 = \frac{Y^2}{2}[J_0{}^2(Y) + J_1{}^2(Y)] \, , \tag{C3}$$

$$I_2 = \frac{Y^2}{2}\left[J_0{}^2(Y) + J_1{}^2(Y) - \frac{2J_0(Y)J_1(Y)}{Y}\right] . \tag{C4}$$

Using the identities $J_0'(y) = -J_1(y)$ and $J_1'(y) = J_0(y) - J_1(y)/y$, we also readily evaluate

$$I_3 = -\tfrac{1}{2}[J_0{}^2(Y) - 1] \, , \tag{C5}$$

and

$$I_4 = \tfrac{1}{2}[1 - J_0{}^2(Y) - J_1^2(Y)] \, . \tag{C6}$$

Substituting the results (C3)–(C6) into equation (C2), and eliminating $J_1(Y)$ by means of equation (12) and B_0 by means of equation (7), we finally obtain the expression given by equation (13).

REFERENCES

Achterberg, A., Blandford, R. D., and Goldreich, P. 1983, *Nature*, **304**, 607.
Baan, W. A. 1980, *Ap. J.*, **239**, 433.
Baberio-Corsetti, P. 1973, *Plasma Phys.*, **15**, 1131.
Benford, G. 1978, *M.N.R.A.S.*, **183**, 29.
Berger, M. A., and Field, G. B. 1984, *J. Fluid Mech.*, **147**, 133.
Bhattacharjee, A., Dewar, R. L., and Monticello. D. A. 1980, *Phys. Rev. Letters*, **45**, 347.
Bicknell, G. V., and Henriksen, R. N. 1980, *Ap. Letters*, **21**, 29.
Bicknell, G. V., and Melrose, D. 1982, *Ap. J.*, **262**, 511.
Blandford, R. D., and Payne, D. G. 1982, *M.N.R.A.S.*, **199**, 883.
Blandford, R. D., and Rees, M. J. 1974, *M.N.R.A.S.*, **169**, 395.
Bodin, H. A. B., and Newton, A. A. 1980, *Nucl. Fusion*, **20**, 1255.
Bridle, A. H., Chan, K. L., and Henriksen, R. N. 1981, *J. R.A.S.* Canada, **75**, 69.
Bridle, A. H., Henriksen, R. N., Chan, K. L., Fomalont, E. B., Willis, A. G., and Perley, R. A. 1980, *Ap. J. (Letters)*, **241**, L145.
Bridle, A. H., and Perley, R. A. 1984, *Ann. Rev. Astr. Ap.*, **22**, 319.
Chan, K. L., and Henriksen, R. N. 1980, *Ap. J.*, **241**, 534.
Chandrasekhar, S. 1969, *Ellipsoidal Figures of Equilibrium* (New Haven: Yale University Press), chaps. 5 and 7.
Chandrasekhar, S., and Kendall, P. C. 1957, *Ap. J.*, **126**, 457.
Cioffi, D. F., and Jones, T. W. 1980, *Ap. J.*, **85**, 368.
Cohn, H. 1983, *Ap. J.*, **269**. 500.
De Young, D. S. 1980, *Ap. J.*, **241**, 81.
Ferrari, A., Trussoni, E., and Zaninetti, L. 1983, *Astr. Ap.*, **125**, 179.
Gardner, F. F., and Whiteoak, J. B. 1966, *Ann. Rev. Astr. Ap.*, **4**, 245.
Gibson, R. D., and Whiteman, K. J. 1968, *Plasma Phys.*, **10**, 1101.
Gradshteyn, I. S., and Ryzhik, I. M. 1965, *Table of Integrals, Series, and Products* (New York: Academic Press).
Hardee, P. E. 1982, *Ap. J.*, **261**, 457.
Henriksen, R. N., Bridle, A. H., and Chan, K. L. 1982, *Ap. J.*, **257**, 63.
Heyvaerts, J. 1981, in *Solar Flare Magnetohydrodynamics*, ed. E. R. Priest (New York: Gordon and Breach), p. 429.
Jacobson, A. R., and Moses, R. W. 1984, *Phys. Rev. A*, **29**, 3335.
Jette, A. D. 1970, *J. Math. Anal. Appl.*, **29**, 109.
Königl, A., and Choudhuri, A. R. 1985, *Ap. J.*, **289**, 188.
Kraichnan, R. H., and Montgomery, D. 1980, *Rept. Progr. Phys.*, **43**, 547.
Laing, R. A., 1981, *Ap. J.*, **248**, 87.
Moffatt, H. K. 1978, *Magnetic Field Generation in Electrically Conducting Media* (Cambridge: Cambridge University Press), chaps. 2 and 3.
Montgomery, D., Turner, L., and Vahala, G. 1978, *Phys. Fluids*, **21**, 757.
Norman, C. A., and Heyvaerts, J. 1983, *Astr. Ap.*, **124**, L1.
Norman, M. L., Smarr, L., Winkler, K.-H. A., and Smith, M. D. 1982, *Astr. Ap.*, **113**, 285.
Perley, R. A., Bridle, A. H., and Willis, A. G. 1984, *Ap. J. Suppl.*, **54**, 291 (PBW).
Rees, M. J., Begelman, M. C., and Blandford, R. D. 1981, *Ann. NY Acad. Sci.*, **375**, 254.
Reiman, A. 1980, *Phys. Fluids*, **23**, 230.
Rusbridge, M. G. 1977, *Plasma Phys.*, **19**, 499.
Tajima, T., and Leboeuf, J. N. 1980, *Phys. Fluids*, **23**, 884.
Taylor, J. B. 1974, *Phys. Rev. Letters*, **33**, 1139.
———. 1975, in *Plasma Physics and Controlled Fusion*, Tokyo 1974 (Vienna: International Atomic Energy Agency), vol. 1, p. 161.
Turner, L. 1983*a*, *Nucl. Instr. Methods*, **207**, 23.
———. 1983*b*, *Ann. Phys.*, **149**, 58.
Turner, L., and Christiansen, J. P. 1981, *Phys. Fluids*, **24**, 893.
Voslamber, D., and Callebaut, D. K. 1962, *Phys. Rev.*, **128**, 2016.
Woltjer, L. 1958, *Proc. Nat. Acad. Sci.*, **44**, 489.

ARNAB RAI CHOUDHURI: Laboratory for Astrophysics and Space Research, University of Chicago, 933 East 56th Street, Chicago, IL 60637

ARIEH KÖNIGL: Astronomy and Astrophysics Center , University of Chicago, 5640 South Ellis Avenue, Chicago, IL 60637